Applied Surface Science 540 (2021) 148397

Contents lists available at ScienceDirect

Applied Surface Science

journal homepage: www.elsevier.com/locate/apsusc

Tunable surface plasmon resonance of Al-Cu bimetallic nanoparticles thin films induced by pulsed-laser

Jing Liao [a], Yuhao Zhan [a], Qingyou Liu [b], Ruijin Hong [a,*], Chunxian Tao [a], Qi Wang [a], Hui Lin [a], Zhaoxia Han [a], Dawei Zhang [a]

[a] Engineering Research Center of Optical Instrument and System, Ministry of Education and Shanghai Key Lab of Modern Optical System, University of Shanghai for Science and Technology, No.516 Jungong Road, Shanghai 200093, China
[b] Key Laboratory of High-temperature and High-pressure Study of the Earth's Interior, Institute of Geochemistry, Chinese Academy of Sciences, Guiyang 550081, China

ARTICLE INFO

Keywords:
LSPR
Bimetallic nanoparticles
Laser irradiation
SERS
FDTD

ABSTRACT

Al-Cu bimetallic nanoparticles (NPs) thin film was fabricated by Nd:YAG fiber pulsed-laser irradiation of Al/Cu bilayers at ambient conditions. The effects of laser irradiation on the morphology, structure, composition and optical properties of the samples were investigated. The tunability of both localized surface plasmon resonance (LSPR) wavelength and intensity were realized by varying the pulse shot or relative thickness of Al/Cu bilayers. The SEM analysis with EDS results further revealed that the obtained particles consisted of a mean diameter of 36–80 nm bimetallic NPs system, being dependent on the Cu proportion. In addition, Surface-enhanced Raman spectroscopy (SERS) measurement and corresponding finite-difference time-domain (FDTD) simulation of before and after laser irradiation samples were discussed to verify the LSPR properties.

1. Introduction

Metal nanoparticles(NPs) have attracted lots of interests in many application areas such as electronic devices [1], solar cell [2], catalysis [3,4], bio-sensors [5,6], Surface-enhanced Raman spectroscopy (SERS) [7,8] and other fields, due to their unique physics-chemical properties and functionalities. Especially, the distinct localized surface plasmon resonance (LSPR) properties of metal NPs is the core of biosensing [9]. When the resonance frequency of the surface conduction electrons and electromagnetic radiation are matched, LSPR induced by the coherent oscillation of conduction electrons shows its high extinction coefficients and significant enhancement of near-field amplitude [10]. This near-field enhancement is also the basic mechanism of SERS and other surface-enhanced spectroscopic processes, which can be effectively used in medical diagnosis. The efficiency and intensity of these applications largely depend on the LSPR properties, especially, the LSPR wavelength, which is determined by the size, shape, local dielectric environment and composition of metal NPs [11]. Hence, by modifying these factors appropriately can achieve a strong tunable LSPR character.

Based on previous research, surface plasmon resonance mainly focus on noble metals such as gold and silver with strong resonant oscillations. Many other metals (i.e., In, Cu, Al, Na and Li) also have this characteristic, and may support LSPR for at least part of the UV–vis-IR region, but little research has been done on these metals [12]. However, for a given shape, these metals have a fixed LSPR, which limits the potential applications of each material [13]. Recently, more attention has turned to bimetallic nanoparticle systems. In addition to the usual size and shape manipulation, the composition change provides another dimension in tailoring metallic NPs properties [14]. The Al-Cu bimetallic system has been widely applied in catalysis and machining due to the improvement of material properties [15], but its optical properties have been rarely studied. The physical properties of Al and Cu vary greatly, and both have some advantages and drawbacks. Al has a broader tunable LSPR wavelength than noble metals, while Cu has stronger LSPR properties and lower optical loss [16,17]. Therefore, it is worth practicing to combine the advantages of Al and Cu with bimetallic NPs to study the optical properties.

In this paper, we propose an alternative cost-effectively method to fabrication of Al-Cu bimetallic NPs by pulsed-laser irradiation at ambient conditions. The surface morphology, roughness and NPs distribution of the Al-Cu bimetallic NPs thin film are dependent on the thickness of Al layer and Cu layer. Both the surface plasmon resonance wavelength and intensity can be tuned effectively by varying either pulse shot or the relative thickness of each layer. The influence of

* Corresponding author.
E-mail address: rjhong@usst.edu.cn (R. Hong).

https://doi.org/10.1016/j.apsusc.2020.148397
Received 23 August 2020; Received in revised form 28 October 2020; Accepted 4 November 2020
Available online 8 November 2020

relative thickness and laser parameters on structure, composition, optical absorption, Raman scattering properties of all samples were investigated.

2. Experiment

Al/Cu bilayer thin films were deposited on fused quartz substrates by electron beam evaporation using sintered Al (99.9%) and Cu (99.9%). The deposition chamber was evacuated to a base pressure less than 4.0×10^{-4} Pa with the deposition rate of 1 Å/s. In this study, the total thickness of the bilayers was controlled at 10 nm monitored by an in situ quartz crystal microbalance. The investigated thickness combinations are Al 10 nm, Al 7 nm/Cu 3 nm, Al 5 nm/Cu 5 nm, Al 3 nm/Cu 7 nm, Cu 10 nm, respectively. Those as-deposition Al/Cu bilayer samples were then irradiated by a Nd :YAG fiber pulsed-laser operating at 1064 nm wavelength with 100 ns pulse width and 55 kHz repetition rate. Here, the pulse energy represents the energy of a single pulse, and the pulse energy density refers to the pulse energy divided by the beam size. The laser output beam (231.5 mJ/cm^2 energy density) of 0.01 mm diameter was made to irradiate the film directly. The large-area dewetting of Al/Cu bilayers was performed by laser line scanning. By varying the laser scanning speed, the average number of laser pulses shot on the per position was controlled. In this experiment, the laser scanning speed increased from 100 to 500 mm/s result in the number of pulse shot of per position reduced from 5 to 1. The schematic diagram of this procedure was shown in Fig. 1.

The surface morphology was analysis by scanning electron microscope (SEM, S-500, ZEISS). The root-mean-square (RMS) roughness of samples was measured by atomic force microscopy (AFM, XE-100, Park System). Elemental analysis was performed by energy-dispersive X-ray spectroscopy (EDS). The optical absorption of the samples was measured by a UV–vis-NIR double beam spectrophotometer (Lambda 1050, Perkins Elmer). The component analysis of the samples was obtained by the Thermo Scientific K-Alpha þ X-ray photoelectron spectroscopy (XPS). Moreover, the Raman scattering spectra were measured with a confocal microprobe Raman system (inVia Raman Microscope, Renishaw) operating at 633 nm wavelength with the power of the laser setting to 3mW. All these measurements were performed at room temperature.

3. Results and discussions

3.1. Surface morphology

Fig. 2(a-f) shows the representative SEM images of Al/Cu bilayer structures before and after laser irradiation. According to Fig. 2(a), as-deposited Al/Cu bilayer film consisted of disorder island-like grains with the range of 10–20 nm. After laser irradiation, Fig. 2(b-d) illustrates how the morphology of bilayers vary with a different structure. Being different from the single-layer structure, the bilayers was transformed into spheroidal or ellipsoidal structures with uneven size distribution, which was closely related to the relative thickness. For Al-rich structure in Fig. 2(c), the film was dewetted into large-sized particles with some smaller particles gathered around. The overall size of the particles increased with the proportion of Cu increasing, as shown in Fig. 2(d). However, for the Cu-rich structure in Fig. 2(e), pulsed-laser irradiation could completely dewetted it into uniform NPs size with the largest contact angle, which has the lowest dewetting threshold. Fig. 2(b) and (f) show the surface morphology of as-irradiated single-layer Al and Cu thin films, respectively. Instead of forming obvious particles, they presented the shape of hills and valleys with a few particles agglomerated, indicating that the films were still in a wet state [18].

Fig. 2(g) shows the particle size distributions of as-irradiated Al/Cu bilayer films measured from SEM images. For as-irradiated Al 7 nm/Cu 3 nm and Al 5 nm/Cu 5 nm samples, the particle size presents a polydisperse distribution with the average particle sizes of 36.35 nm and 77.64 nm, respectively. Both smaller particle and large-sized particle groups appear in the diameter distribution chart. However, in the Cu-rich sample, the particle size presents a monodisperse distribution with the average particle size of 80.82 nm. With the proportion of Cu increasing, the particle size gradually increases and the distribution concentrates. Fig. 2(h) shows the values of the root mean square (RMS) surface roughness of samples with Al thickness increased before and after laser irradiation. The RMS values of as-deposited samples and as-irradiated samples are 1.712, 1.480, 1.097, 1.375, 1.738 nm and 3.503, 7.513, 5.657, 4.661, 10.558 nm, respectively. In bilayer structures, with the increase of Cu layer thickness, the size of particles increased correspondingly and the surface of bilayers become rougher, resulting in a higher value of RMS. Fig. 2(i) shows the relationship between RMS values and pulse shot number of per position. With the number of pulse shot increasing, it promoted the dewetting behavior,

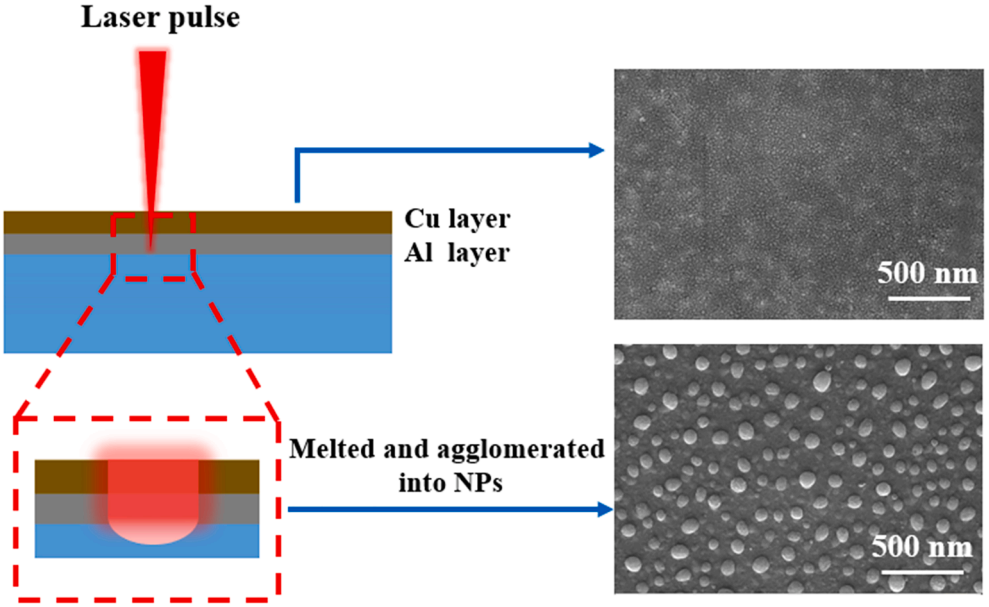

Fig. 1. Schematic diagram of the formation of Al-Cu bimetallic NPs.

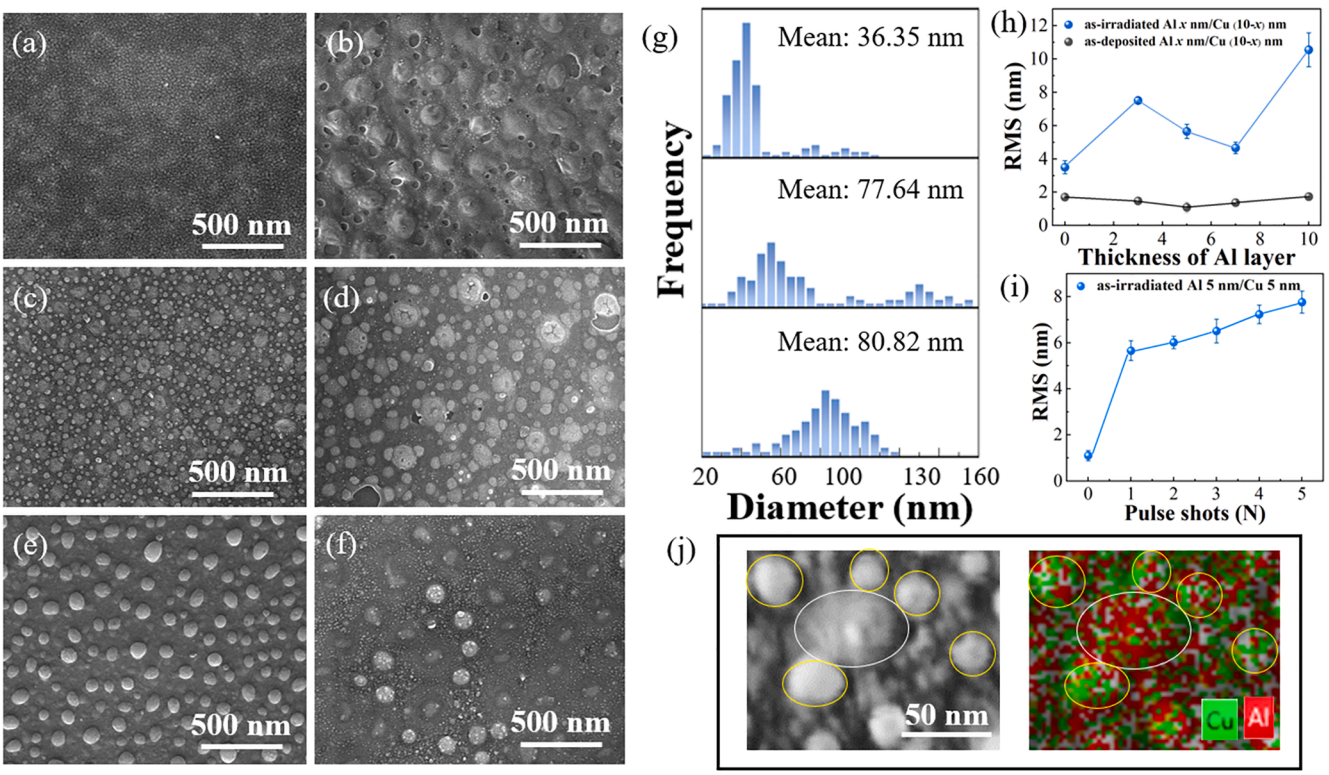

Fig. 2. SEM images of as-deposited (a) Al 5 nm/Cu 5 nm sample; as-irradiated (b) Al 10 nm, (c) Al 7 nm/Cu 3 nm, (d) Al 5 nm/Cu 5 nm, (e) Al 3 nm/Cu 7 nm and (f) Cu 10 nm samples with single pulse shot of per position. (g) Particle size distributions charts of as-irradiated Al 7 nm/Cu 3 nm (upper chart), Al 5 nm/Cu 5 nm (middle chart) and Al 3 nm/Cu 7 nm (lower chart) samples. (h) the RMS value of samples with Al thickness increased; (i) the RMS value of Al 5 nm/Cu 5 nm bilayer with the number of pulse shot increased. (j) SEM and mapping image of as-irradiated Al 5 nm/Cu 5 nm bilayer.

which also results in an increasing of RMS value [14].

Fig. 2(j) shows the SEM and mapping image of a typical particle group of as-irradiated Al 5 nm/Cu 5 nm bilayer to reveal the particle composition of the Al/Cu bilayers after laser irradiation, which is consistent with the particle structure in Fig. 2(d). Elemental analysis carried out by EDS revealed that pulsed-laser induced NPs are not a perfect mixture of the two elements, but Al-rich (white circle) and Cu-rich (yellow circle) NPs emerged. There is a large melting point difference between Al and Cu (Al = 660 °C, Cu = 1085 °C), and the lattice constants of Al and Cu are different to one another (Al = 4.05 Å, Cu = 3.61 Å). This makes it difficult for as-irradiated Al/Cu bilayers to form single-phase alloys. In addition, the processes of rapid heating and cooling were not sufficient for the diffusion of Al and Cu atoms, and the solubility of Cu in Al decreased sharply with the temperature decreasing [19]. This leads to the formation of Al-rich and Cu-rich particles containing only a few per cent of the other metal, and the nature of these two particles are nearly pure Al and Cu particles. The composite nanostructure of smaller Cu-rich NPs and large-sized Al-rich NPs constitutes the mixed bimetallic NPs system.

In the process of laser irradiation, the main effect on the samples is the absorption of laser radiation in the material, which converts the electronic energy derived from incident laser beam into the heat and promotes atoms aggregation [20]. Al layer, as a buffer layer in the bilayer structure, can promotes the overall heat conduction and reshaping due to its low melting point, soft texture and good thermal conductivity [21]. Consequently, there is a lower pulsed energy threshold required for bilayer structure to be dewetted into NPs. Besides, pulsed-laser irradiation process has ablation effect of leading to the material loss, and simply increasing the laser energy to achieve dewetting is not desirable. As a result, it is a feasible method to induce dewetting by using the low melting point characteristic of the Al/Cu bilayer layer structure.

3.2. Composition and valence state

Fig. 3 shows the XPS spectra of the samples before and after laser irradiation with evident signals of Al 2p and Cu 2p at 75.1, 933.6 and 955.8 eV, respectively. These results are similar to those reported by others [22–24]. According to Fig. 3(a) of high-resolution Cu 2p spectra, two peaks appeared at 932.7 and 934.8 eV, which were corresponding to Cu_2O and CuO respectively. For Cu 2p1/2, there also exist two peaks: one peak located at 952.5 eV was assigned to metallic Cu, the other band appearing at 954.4 eV belonged to CuO. A satellite peak at 942.9 eV for characteristic Cu^{2+} was also observed [25]. According to Fig. 3(a), both CuO and Cu_2O were detected due to the surface oxidation of as-deposited Al/Cu bilayer in ambient conditions. Fig. 3(c) shows the Cu 2p spectra of as-irradiated Al 5 nm/Cu 5 nm bilayers with pulse shot number of 1, 3 and 5 of per position, respectively. The results demonstrated the coexistence of Cu, Cu_2O and CuO in the Al/Cu bilayers, indicating that appreciable oxidation occurred during laser irradiation. The characteristic peaks of Cu 2p3/2 belonging to Cu_2O exhibited higher in intensity and shift to a lower energy position from 932.71 eV to 932.45 eV with the increase of pulse shot. The obvious change resulted from a charge imbalance which was induced by the oxidation reaction in the case of laser thermal effect [26]. Fig. 3(e) and (g) show the Cu 2p spectra of as-irradiated samples with different thickness combinations. The relative ratios of the corresponding Cu components were listed in Table 1. The Cu^0 content of as-irradiated samples (19.1%) was higher than that of the deposited sample (10%). This may be caused by the strong reducibility of metal Al under high temperature conditions. The pulse shot number affects the valence state of Cu. The content of Cu^{2+} increased with higher pulse shot number, while the content of Cu^+ and Cu^0 decreased slightly.

Fig. 3(b-h) show the Al 2p spectra of Al/Cu bilayers before and after laser irradiation. The shape of those spectra was featured by a strong

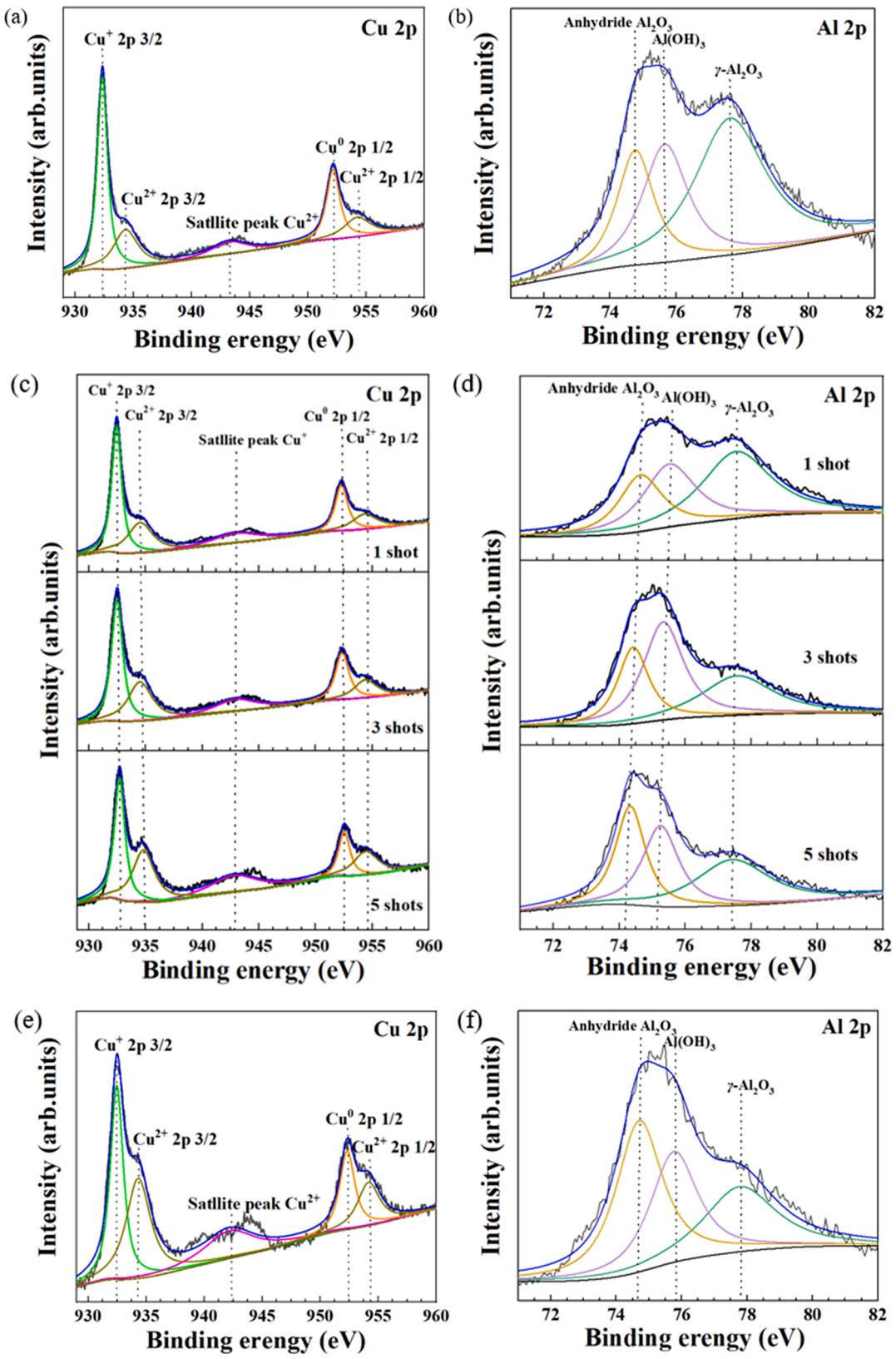

Fig. 3. The XPS spectra for Cu 2p and Al 2p region of (a-b) as-deposited Al 5 nm/Cu 5 nm bilayer, (c-d) as-irradiated Al 5 nm/Cu 5 nm samples with increased number of pulse shot, (e-f) as-irradiated Al 7 nm/Cu 3 nm and (g-h) as-irradiated Al 7 nm/Cu 3 nm samples with single pulse shot.

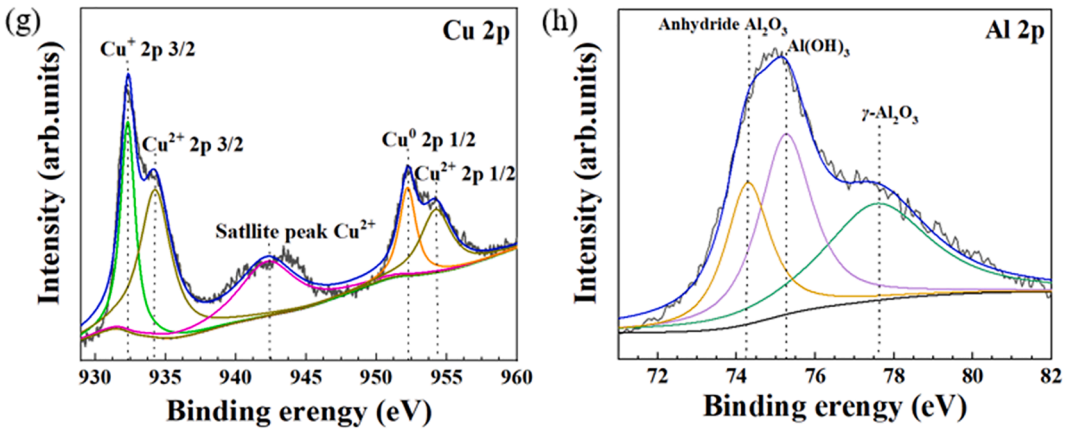

Fig. 3. (*continued*).

Table 1
Relative ratio of Cu components with different thickness combination and laser pulse shot calculated from the XPS of Cu 2p Spectra.

Samples	Cu^{2+}(%)	Cu^{+}(%)	Cu^{0}(%)
Al 5 nm/Cu 5 nm (0 shot)	43.7%	46.3%	10%
Al 5 nm/Cu 5 nm (1 shot)	38.4%	42.5%	19.1%
Al 5 nm/Cu 5 nm (3 shots)	40.2%	41.2%	18.6%
Al 5 nm/Cu 5 nm (5 shots)	48.8%	36.9%	14.3%
Al 7 nm/Cu 3 nm (1 shot)	50.1%	33.5%	16.4%
Al 3 nm/Cu 7 nm (1 shot)	60.2%	26.7%	13.1%

peak at about 75 eV and a weak peak at about 78 eV, which was marked as, respectively. By means of Gaussian fitting, the strong peak can be divided into two peaks. According to Fig. 3(b), the fitting XPS Al 2p spectra show three peaks located at 74.6, 75.6 and 77.6 eV that are assigned to γ-Al_2O_3, $Al(OH)_3$ and anhydride Al_2O_3, respectively [24]. As can be seen, the detected Al on the surface of the samples was completely activated to form Al-O-related chemical bonds. Both the relative thickness of Al/Cu bilayers and pulse shot number have the effect on the elemental chemical state of Al. The binding energies of Al in the fitted XPS spectra of Al/Cu bilayers varied with the pulse shot number of per position, and all the peaks showed the shift to the higher binding energy, as shown in Fig. 3(d).

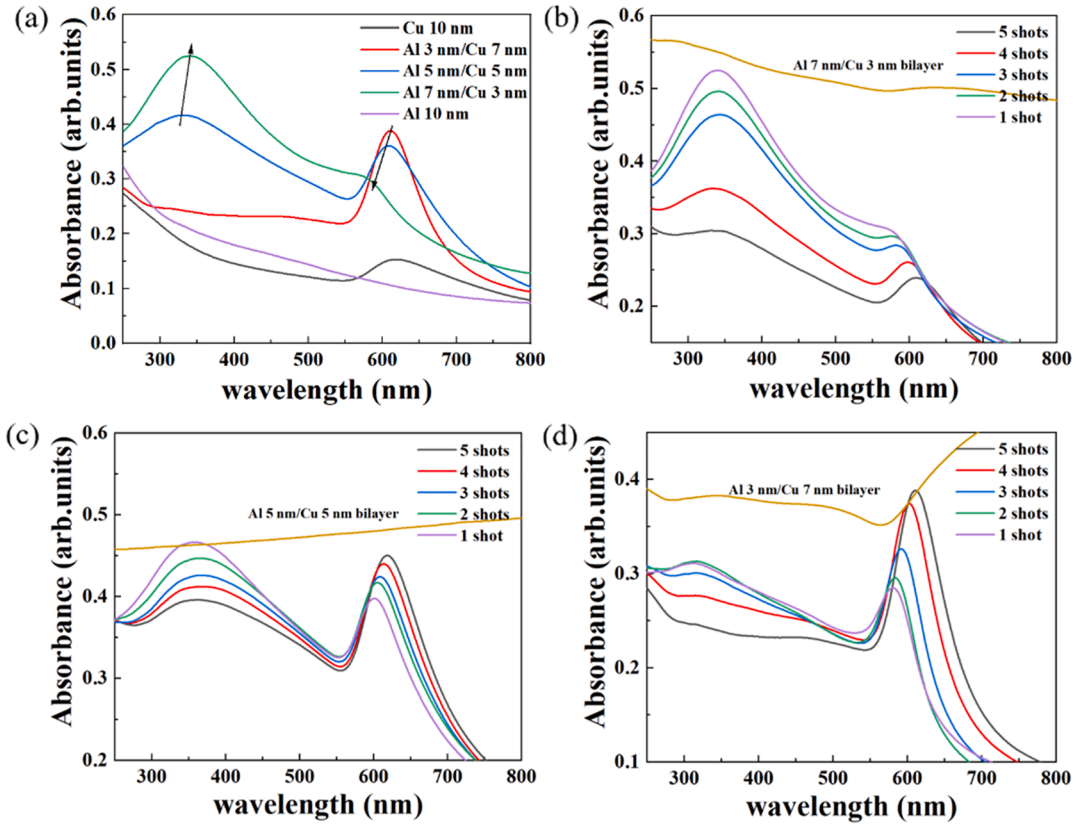

Fig. 4. Absorption spectra of as-irradiated (a) Al/Cu bilayers with various structural thickness; as-irradiated (b) Al 7 nm/Cu 3 nm, (c) Al 5 nm/Cu 5 nm and (d) Al 3 nm/Cu 7 nm samples with the increasing of pulse shot number.

3.3. Optical characterization

Fig. 4 shows the optical absorption spectra of Al/Cu bilayers with different relative thicknesses and laser parameters. According to Fig. 4 (a), for the single layer structure, a weak broad peak was observed in as-irradiated Cu thin film, while no obvious absorption peak was detected in the as-irradiated Al thin film. However, for the bilayer structure samples, unique LSPR characteristics appeared after laser irradiation. In the as-irradiated Al 7 nm/Cu 3 nm and Al 5 nm/Cu 5 nm samples with mixed bimetallic NPs system, two distinct absorption peaks located at around 330 nm and 610 nm were detected in absorption spectra, corresponding to Al and Cu NPs [27–29], respectively. It is to mention that the Al-rich and Cu-rich NPs do not exhibit obviously interparticle coupling in the mixed system. The LSPR peaks show slight shift with the proportion variation, and their intensity is positively correlated to the proportion of mixing [30]. In this composite bimetallic NPs system, the particles does not affect the LSPR peak of each other, and hence their absorption spectra are the simple addition of the spectra of their individual monometals i.e. pure Al or pure Cu NPs. The relative thickness of the Al/Cu bilayers determines the composition of the mixed bimetallic NPs system and LSPR peak intensity. The two peaks structures in the absorption spectra also indicate the formation of the mixed system. However, for the absorption spectra of Cu-rich sample, the particle size distribution was monodisperse and did not form a composite bimetallic NPs system like Al-rich sample, only a single LSPR peak of Cu NPs was detected with sharp peak while the characteristic of Al NPs was significantly suppressed.

The optical absorption spectra as shown in Fig. 4(b-d) reveal the influence of the number of laser pulse shot on samples. No obvious absorption peaks are observed in the as-deposited samples due to the continuous film structure[8]. During the laser irradiation, the number of laser pulse shot determined the heating cycle of per position and influence the dewetting behavior of the irradiated area, which directly affects the LSPR characteristic of the samples. For the Al-rich structure (as shown in Fig. 4(b)), the LSPR characteristic of Al NPs is much stronger than that of Cu NPs. The increase in the number of pulse shot would promote the aggregation of the metal atoms, resulting in larger particle spacing and form more regular NPs with slight increase in size. For Cu-rich particles, with increasing number of pulse, which has higher absorption cross-sections, the slight red shift and the enhancement of LSPR peak were observed [31]. The oxidation of Cu does not significantly affect its LSPR characteristics. For the Al-rich particles, there is Al oxidation on the surface. With the pulse number increasing, the LSPR characteristic was suppressed by the oxidation of Al [32]. Hence, the intensity of the Al LSPR peak decreased correspondingly. This phenomenon appeared in the Al 5 nm/Cu 5 nm and Al 3 nm/Cu 7 nm bilayers (Fig. 4(c-d)), which realizes the transfer and the tuning of LSPR characteristics between Al and Cu NPs. It is obvious that the LSPR characteristic of Al-Cu bimetallic NPs thin film is affected by laser processing parameters and structural thickness, which essentially changes the particle composition and diameter distribution. Therefore, the tunable LSPR properties can be achieved by controlling the structural

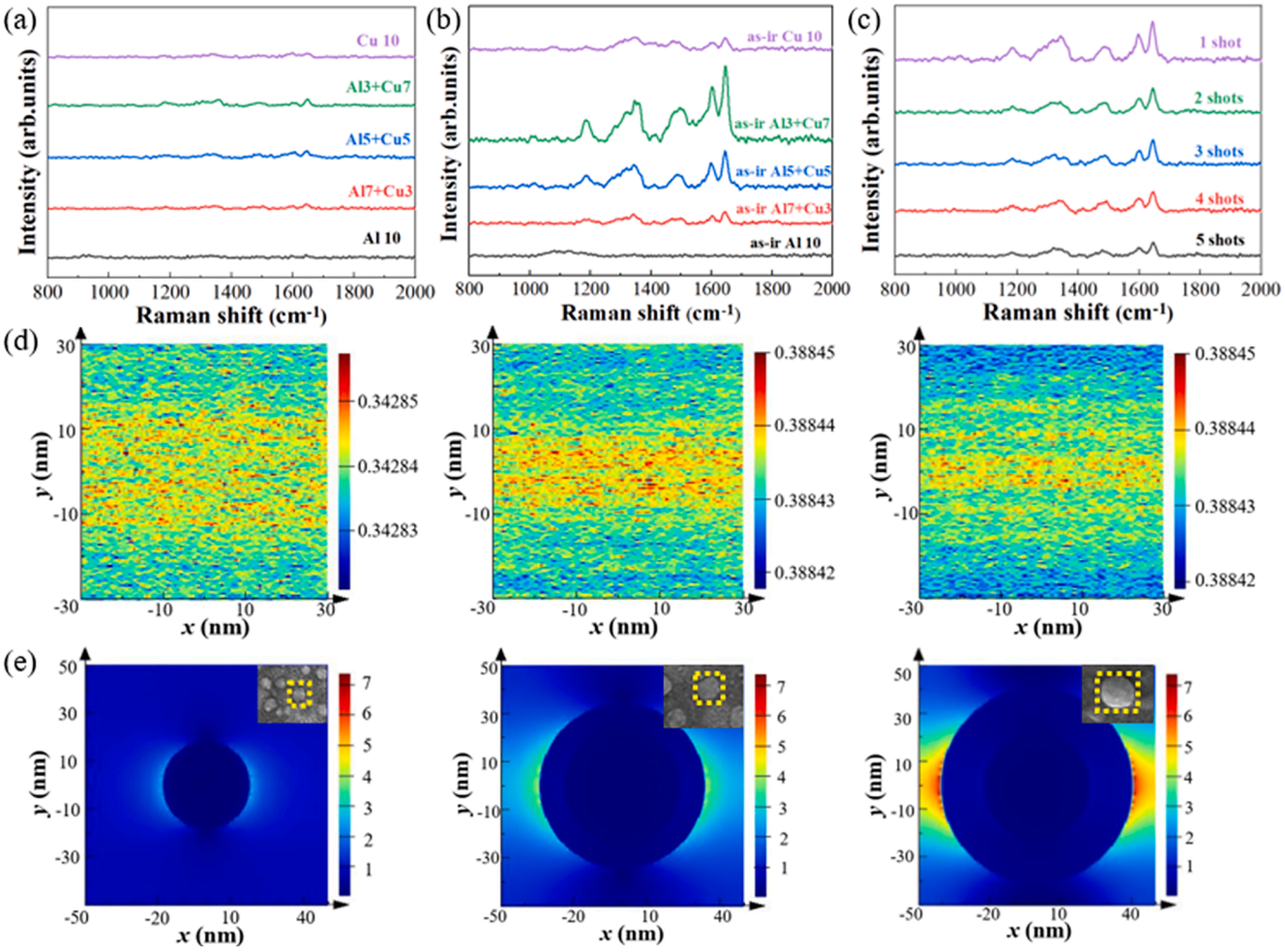

Fig. 5. Raman scattering spectra of R6G on the (a) as-deposited and (b) as-irradiated Al/Cu bilayers with different thickness combinations and (c) as-irradiated Al 5 nm/Cu 5 nm bilayer with increased number of pulse shot; FDTD simulated electric field amplitude patterns for (d) as-deposited Al/Cu bilayers and (e) Al-Cu bimetallic NPs with the thickness of Cu layer increasing.

thickness of Al/Cu bilayers and manipulating laser irradiation parameters [33].

3.4. SERS performance

As a demonstration of the potential application of tunable LSPR absorption, the Al-Cu bimetallic NPs thin film was used as SERS substrates for probing the Rhodamine 6G (R6G) molecule with the concentration of 10^{-4} mol/L, as shown in Fig. 5(a-c). To reduce the fluorescence effect, excitation light with a wavelength of 633 nm was used to operate the Raman scattering measurement, which is also close to the LSPR peak of Cu NPs. There are three strongest Raman peaks of R6G located at about 1645, 1599 and 1360 cm^{-1} are observed, corresponding to the stretching vibration mode of aromatic C-C [11]. For the as-deposited samples in Fig. 5(a), no obvious Raman signal was detected. While in as-irradiated samples showed obvious enhancement in Raman intensity, as shown in Fig. 5(b). Especially for the Al/Cu bilayer structure, with the proportion of Cu increasing, the Raman scattering signal intensity of the R6G molecule significantly was enhanced. Fig. 5 (c) illustrates the influence of the pulse shot number on the intensity of Raman signals. With the number of pulse shot increasing, the Raman signal intensity of the samples show a decrease trend.

The basic of enhancement theory of Raman scattering signal from a SERS substrate includes two parts: electromagnetic theory and chemical theory [34]. The SERS activity of metal material is derived from both electromagnetic and chemical enhancement [35]. Therefore, the absorption spectra of the samples could be discussed together with SERS [36]. According to Fig. 4(a), with the proportion of Cu increasing, the absorption intensity of the LSPR peak increases and shows a shift towards short wavelength which is closed to the excitation wavelength, resulting in a better SERS performance. While with the decrease of the number of pulse shot of per position which can suppresses the dewetting behavior of the bilayers, resulting in a slight decrease in particle size but a denser distribution, and causes more “hot spot” to excite the local electrical fields [16]. On the other hand, laser irradiation can induce the formation of oxygen vacancies and generate parts of Cu_2O component on the particle surface. With the number of pulse shot decreasing, the content of Cu_2O also increases which is consistent with the results in Table 1. Cu_2O will recombine with the detection molecule to generate charge-transfer and interact with the detection laser to cause the enhancement of the SERS signal [37]. Although the LSPR characteristics in Fig. 4(c) was enhanced with the increase of pulse shot number, the SERS performance was still reduced.

To further verify those points above, the FDTD method was used to calculate the electromagnetic field distribution of Al/Cu bilayer thin films before and after laser irradiation, as shown in Fig. 5(d-e). In this simulation, a 633 nm laser irradiated perpendicularly to the x-y plane of the samples with the polarization along the y-axis direction, the diameter of Al-Cu bimetallic NPs is based on the average particle diameter calculated by SEM images. According to Fig. 5(d), the electric field distribution is uniform, and the intensity is weak for the as-deposited samples due to the smooth surface. while the as-irradiated samples exhibits enhancements in electric field intensity, which is consistent with the SERS performance, as shown in Fig. 5(e). The “hot spots” formed on the localized surface between the spacing of NPs lead to the enhanced electric field. Moreover, the electric field intensity increases significantly with the larger diameter of NPs and the increased Cu content. These simulation results are consistent well with the experimental results above, proving that the Al-Cu bimetallic NPs thin film features significant LSPR performance improvement.

4. Conclusion

In this study, we investigated the structure and optical properties of Al/Cu bilayer films modified by laser irradiation. The results showed that the Al/Cu bilayer structure significantly could reduce the dewetting threshold compared that of the single-layer Al or Cu film, forming a mixed bimetallic NPs system. In particular, the LSPR properties can be modulated by varying either the relative thickness or the pulse shot number to achieve the wavelength shift and the intensity variation of surface plasmon in the Al-Cu bimetallic NPs thin film. Additionally, the SERS performance was demonstrated by and FDTD simulation. In summary, this study provides a simple and cost-effective method to fabricate bimetallic NPs with tunable LSPR properties.

CRediT authorship contribution statement

Jing Liao: Writing - original draft. **Yuhao Zhan:** Software. **Qingyou Liu:** Investigation. **Ruijin Hong:** Review, Supervision. **Chunxian Tao:** Data curation, Formal analysis. **Qi Wang:** Data curation. **Hui Lin:** Data curation. **Zhaoxia Han:** Software. **Dawei Zhang:** Validation.

Declaration of Competing Interest

The authors declare that they have no known competing financial interests or personal relationships that could have appeared to influence the work reported in this paper.

Acknowledgement

This work was partially supported by the National Natural Science Foundation of China (61775140, 61775141, and 62075133)

Appendix A. Supplementary data

Supplementary data to this article can be found online at https://doi.org/10.1016/j.apsusc.2020.148397.

References

[1] S. H., K. ParkHeng, PanCostas, P. GrigoropoulosAlbert, P. PisanoChristine, K. LuscombeJean, M.J. Fréchet, Direct Nanoimprinting of Metal Nanoparticles for Nanoscale Electronics Fabrication, Nano Letters 7 (2007).
[2] S. Mokkapati, F.J. Beck, A. Polman, K.R. Catchpole, Designing periodic arrays of metal nanoparticles for light-trapping applications in solar cells, Appl. Phys. Lett. 95 (5) (2009) 053115, https://doi.org/10.1063/1.3200948.
[3] C. Deng, R. Hong, M. Jing, J. Shi, T. Yan, C. Tao, D. Zhang, Photocatalytic performance of TiO2 thin film decorated with Cu2O nanoparticles by laser ablation, Optical Materials 94 (2019) 130–137.
[4] R.M. Crooks, M. Zhao, L. Sun, V. Chechik, L.K. Yeung, Dendrimer-Encapsulated Metal Nanoparticles: Synthesis, Characterization, and Applications to Catalysis, Accounts of Chemical Research 34 (2001) 181.
[5] A.J. Haes, S. Zou, G.C. Schatz, R.P.V. Duyne, Nanoscale Optical Biosensor: Short Range Distance Dependence of the Localized Surface Plasmon Resonance of Noble Metal Nanoparticles, The Journal of Physical Chemistry B 108 (2004).
[6] Y. Hu, H. Cheng, X. Zhao, J. Wu, F. Muhammad, S. Lin, J. He, L. Zhou, C. Zhang, Y. u. Deng, P. Wang, Z. Zhou, S. Nie, H. Wei, Surface-Enhanced Raman Scattering Active Gold Nanoparticles with Enzyme-Mimicking Activities for Measuring Glucose and Lactate in Living Tissues, ACS Nano 11 (6) (2017) 5558–5566.
[7] A. Philip, B. Ankudze, T.T. Pakkanen, A simple one-step fabrication of gold nanoparticles-based surface-enhanced Raman scattering substrates using rice grains, Applied Surface Science 480 (2019) 229–234.
[8] R. Hong, W. Sun, Q. Liu, Z. Li, C. Tao, D. Zhang, D. Zhang, Al-induced tunable surface plasmon resonance of Ag thin film by laser irradiation, Appl. Phys. Express 12 (8) (2019) 085503, https://doi.org/10.7567/1882-0786/ab2c30.
[9] J.N. Anker, W.P. Hall, O. Lyandres, N.C. Shah, J. Zhao, R.P.V. Duyne, Biosensing with plasmonic nanosensors, Nanoscience and Technology 7 (2010) 308.
[10] K.A. Willets, R.P. Van Duyne, Localized Surface Plasmon Resonance Spectroscopy and Sensing, Annu. Rev. Phys. Chem. 58 (1) (2007) 267–297.
[11] C. Yang, C. Zhang, Y. Huo, S. Jiang, H. Qiu, Y. Xu, X. Li, B. Man, Shell-isolated graphene@Cu nanoparticles on graphene@Cu substrates for the application in SERS, Carbon 98 (2016) 526–533.
[12] W. Wei, R. Hong, Y. Meng, C. Tao, D. Zhang, Electron-beam irradiation induced phase transformation, optical absorption and surface-enhanced Raman scattering of Indium tin alloy thin films, Superlattices and Microstructures 106 (2017) 189–196.
[13] K. Lance Kelly, Eduardo Coronado, Lin Lin Zhao, G.C. Schatz*, The Optical Properties of Metal Nanoparticles: The Influence of Size, Shape, and Dielectric Environment, The Journal of Physical Chemistry B 107 (2003).
[14] Yoonseok Oh, Jeeyoung Lee, Myeongkyu Lee, Fabrication of Ag-Au bimetallic nanoparticles by laser-induced dewetting of bilayer films, Applied Surface Science 434 (2018) 1293–1299.

[15] Farhad Larki, Alam Abedini, Md. Shabiul Islam, Sahbudin Shaari, Sawal Hamid Md Ali, P. Susthitha Menon, Azman Jalar, Elias Saion, Jahariah Sampe, Burhanuddin Yeap Majlis, Structural phase transformations in radiolytically synthesized Al–Cu bimetallic nanoparticles, J Mater Sci 50 (12) (2015) 4348–4356.
[16] Ruijin Hong, Wen Shao, Wenfeng Sun, Cao Deng, Chunxian Tao, Dawei Zhang, Laser irradiation induced tunable localized surface plasmon resonance of silver thin film, Optical Materials 77 (2018) 198–203.
[17] T.F. Villesen, C. Uhrenfeldt, B. Johansen, J.L. Hansen, H.U. Ulriksen, A.N. Larsen, Aluminum nanoparticles for plasmon-improved coupling of light into silicon, Nanotechnology 23 (2012), 085202.
[18] S.J. Henley, J.D. Carey, S.R.P. Silva, Pulsed-laser-induced nanoscale island formation in thin metal-on-oxide films, Physical Review B 72 (2005).
[19] Shuming Chen, Haiyan Wang, Huiping Ren, Xueyun Gao, Zhaofeng Yao, First-principles study of phase stability and solubility in Al-(Cu, Zr) alloys, Ferroelectrics 523 (1) (2018) 112–118.
[20] Haribabu Palneedi, Jung Hwan Park, Deepam Maurya, Mahesh Peddigari, Geon-Tae Hwang, Venkateswarlu Annapureddy, Jong-Woo Kim, Jong-Jin Choi, Byung-Dong Hahn, Shashank Priya, Keon Jae Lee, Jungho Ryu, Laser Irradiation of Metal Oxide Films and Nanostructures: Applications and Advances, Adv. Mater. 30 (14) (2018) 1705148, https://doi.org/10.1002/adma.201705148.
[21] Shang-Nan Chou, Horng-Hwa Lu, Ding-Fwu Lii, Jow-Lay Huang, Processing and physical properties of Al2O3/aluminum alloy composites, Ceramics International 35 (1) (2009) 7–12.
[22] Lele Lu, Xinxin Xu, Jiaming Yan, Fa-Nian Shi, Yuqiu Huo, Oxygen vacancy rich Cu 2 O based composite material with nitrogen doped carbon as matrix for photocatalytic H 2 production and organic pollutant removal, Dalton Trans. 47 (6) (2018) 2031–2038.
[23] J. P. Espinós, * J. Morales, A. Barranco, A. Caballero, J. P. Holgado, A.R. González-Elipe, Interface Effects for Cu, CuO, and Cu2O Deposited on SiO2 and ZrO2. XPS Determination, American Chemical Society 106 (2002).
[24] A. Barrera, F. Tzompantzi, J. Campa-Molina, J.E. Casillas, R. Pérez-Hernández, S. Ulloa-Godinez, C. Velásquez, J. Arenas-Alatorre, Photocatalytic activity of Ag/Al2O3–Gd2O3 photocatalysts prepared by the sol–gel method in the degradation of 4-chlorophenol, RSC Advances 8 (2018) 3108–3119.
[25] S. Li, M. Wang, C. Li, J. Liu, M. Xu, J. Liu, J. Zhang, CuxO self-assembled mesoporous microspheres with effective surface oxygen vacancy and their room temperature NO2 gas sensing performance, Science China Materials 61 (2018) 1085–1094.
[26] Mingyuan Zhu, Zihao Zhang, Min Zhong, Muhammad Tariq, Ying Li, Wenxian Li, Hongming Jin, Katerina Skotnicova, Yibing Li, Oxygen vacancy induced ferromagnetism in Cu-doped ZnO, Ceramics International 43 (3) (2017) 3166–3170.
[27] P.K. Khanna, S. Gaikwad, P.V. Adhyapak, N. Singh, R. Marimuthu, Synthesis and characterization of copper nanoparticles, Materials Letters 61 (25) (2007) 4711–4714.
[28] Y. Ekinci, H.H. Solak, J.F. Löffler, Plasmon resonances of aluminum nanoparticles and nanorods, Journal of Applied Physics 104 (2008).
[29] Jérôme Martin, Julien Proust, Davy Gérard, Jérôme Plain, Localized surface plasmon resonances in the ultraviolet from large scale nanostructured aluminum films, Opt. Mater. Express 3 (7) (2013) 954, https://doi.org/10.1364/OME.3.000954.
[30] Probodh K. Kuiri, Tailoring localized surface plasmons in Ag–Al alloys' nanoparticles, Journal of Alloys and Compounds 826 (2020) 154250, https://doi.org/10.1016/j.jallcom.2020.154250.
[31] Ru.G. Nikov, N.N. Nedyalkov, P.A. Atanasov, D. Hirsch, B. Rauschenbach, K. Grochowska, G. Sliwinski, Characterization of Ag nanostructures fabricated by laser-induced dewetting of thin films, Applied Surface Science 374 (2016) 36–41.
[32] Yi Wei, Yu Gu, Mingyou Zhao, Yuhang Dong, Jun Chen, Haibo Zeng, Deep-Ultraviolet Plasmon Resonances in Al-Al 2 O 3 @C Core–Shell Nanoparticles Prepared via Laser Ablation in Liquid, ACS Appl. Electron. Mater. 2 (3) (2020) 802–807.
[33] Wenfeng Sun, Ruijin Hong, Qingyou Liu, Zhengwang Li, Jingqi Shi, Chunxian Tao, Dawei Zhang, SERS-active Ag–Al alloy nanoparticles with tunable surface plasmon resonance induced by laser ablation, Optical Materials 96 (2019) 109298, https://doi.org/10.1016/j.optmat.2019.109298.
[34] H. Dizajghorbani Aghdam, S. Moemen Bellah, R. Malekfar, Surface-enhanced Raman scattering studies of Cu/Cu2O Core-shell NPs obtained by laser ablation, Spectrochim Acta A Mol Biomol Spectrosc 223 (2019), 117379.
[35] John R. Lombardi, Ronald L. Birke, A Unified Approach to Surface-Enhanced Raman Spectroscopy, J. Phys. Chem. C 112 (14) (2008) 5605–5617.
[36] Ruijin Hong, Xianhai Wang, Jialin Ji, Chunxian Tao, Daohua Zhang, Dawei Zhang, ITO induced tunability of surface plasmon resonance of silver thin film, Applied Surface Science 356 (2015) 701–706.
[37] Jie Lin, Yang Shang, Xiaoxia Li, Jian Yu, Xiaotian Wang, Lin Guo, Ultrasensitive SERS Detection by Defect Engineering on Single Cu 2 O Superstructure Particle, Adv. Mater. 29 (5) (2017) 1604797, https://doi.org/10.1002/adma.201604797.